Separation Science and Technology
Publication details, including instructions for authors and subscription information:
http://www.informaworld.com/smpp/title~content=t713708471

Statistical Models to Describe the Structure of Porous Ceramic Membranes

J. H. F. Lim[a]; X. Jia[a]; R. Jafferali[a]; G. A. Davies[a]
[a] Department of Chemical Engineering UMIST Manchester, England

To cite this Article Lim, J. H. F. , Jia, X. , Jafferali, R. and Davies, G. A.(1993) 'Statistical Models to Describe the Structure of Porous Ceramic Membranes', Separation Science and Technology, 28: 1, 821 — 854
To link to this Article: DOI: 10.1080/01496399308019523
URL: http://dx.doi.org/10.1080/01496399308019523

SEPARATION SCIENCE AND TECHNOLOGY, 28(1-3), pp. 821-854 (1993)

STATISTICAL MODELS TO DESCRIBE THE STRUCTURE OF POROUS CERAMIC MEMBRANES

J.H.F. Lim, X Jia, R Jafferali and G A Davies
Department of Chemical Engineering
UMIST
Manchester, England, M60 1QD

ABSTRACT

A knowledge of the material structure of porous membranes is essential in the computation of flux–pressure differential and blinding behavior. The data provided by manufacturers on the internal pore properties, mercury porosimetry and air permeability, is of limited use since it is based for interpretation on an assumed matrix of cylindrical pores. Ceramic membranes are considered in this work for which three different types are investigated. None of these show any resemblance to structures assumed for an interpretation of this data.

The pore structure in all examples vary and it is concluded that deterministic models to describe this are not valid.

Statistical models based on random division of 2 and 3 dimensional space are proposed to describe the structure of cellular ceramic membranes (2 space model), sintered ceramic membranes and foam membranes (3 dimensional space models). The models are shown to be inter–related providing a direct comparison between the membrane structures.

The structures proposed by the models are compared and agree well with experimental data.

INTRODUCTION

In almost all applications of porous membranes it is important to have quantitative knowledge on the pore properties, particularly the free

volume, and pore dimensions. Manufacturers often quote data for air permeability, mercury porosimetry in terms of mercury ingress at various applied pressures, and bubble point data. In order to obtain information on the pore diameters from either mercury porosimetry measurements or air permeability, equations must be applied which invoke some model for the pore structure. Almost all such models assume that the pores are parallel cylindrical pores or are interconnected cylindrical pores. If we examine typical ceramic membranes these assumptions are quite erroneous. The pore structure bears no resemblance at all to either parallel or interconnected cylindrical pores. Knowledge of the bubble point at particular pressures is of little use in determining the pore structure. At best it can give some information on the diameters of pores at one face of the membrane, the face at which the bubble points were measured. Even this interpretation requires an assumption on the cross sectional shape of the pore at the outlet face. Most models assume that this cross section is circular. In this paper we will consider three different types of ceramic membranes which are used in micro and ultra filtration applications. These examples include cellular ceramic membranes. These are typically used in applications at the boundary between ultra and micro filtration. The cut–off pore diameter quoted by the manufactures is between 0.1–4 microns. A second type of ceramic membrane is a sintered ceramic membrane. These are used mainly in micro filtration applications. Finally, the third type considered is a cellular foam membrane which is principally used in micro filtration applications. These types have been chosen since the pore structure in each type of membrane is different. A stochastic model is presented to describe the pore structure in each case. It is shown that these models are all inter–related and can follow logically from one another.

EXPERIMENTAl OBSERVATIONS ON THE STRUCTURE OF CERAMIC MEMBRANES

We will consider the three types of membranes, viz

i) Cellular ceramic membranes,

ii) Sintered ceramic membranes,
iii) Cellular foam membranes.

separately. In each case samples of the various membranes were taken and thin sections made by first impregnating the pore structure with a wax. This was used to support the membrane during sectioning. The membrane was then sectioned carefully using a microtome. Each section was then placed on a slide, this was heated and the wax removed from the section. The section was then prepared for scanning electron microscopy and photomicrographs were then obtained. The magnifications used varied to suit the particular membrane section being studied.

Cellular Ceramic Membranes

A scanning electron micrograph of a typical cellular membrane is shown in Figure 1. The dark areas in the photograph are the pores of the membrane. The actual membrane shown here is an Anotec cellular membrane which has a nominal pore rating of 0.2 μm. This membrane is produced by electrolytic oxidation of aluminum. The cellular structure of the anodic film is the result of local current density at the metal interface. This is not uniform either in spacial distribution or intensity so that an irregular cell pattern is formed. The important feature of this membrane, the type shown here, is that the individual pores whilst irregular in cross section are non–connected, that is they pass through the membrane in the direction perpendicular to the plane shown (z direction)
without connecting to any neighbours. Two types are possible, one in which the pore cross section area is constant in the direction through the membrane, the second type is where the cross section is smaller at one face than the other. The first type is a symmetric membrane and the second type is an asymmetric membrane which is produced by regulating the current density during the growth of the film. If one studies the SEM photograph shown in Figure 1, it can be seen that the individual pores have the shape of an irregular polygon. These fully tessellate the plane shown in the photograph. Because of the non–connectivity of the pores, the structure can be described in 2 dimensional space. This is true for symmetric membranes

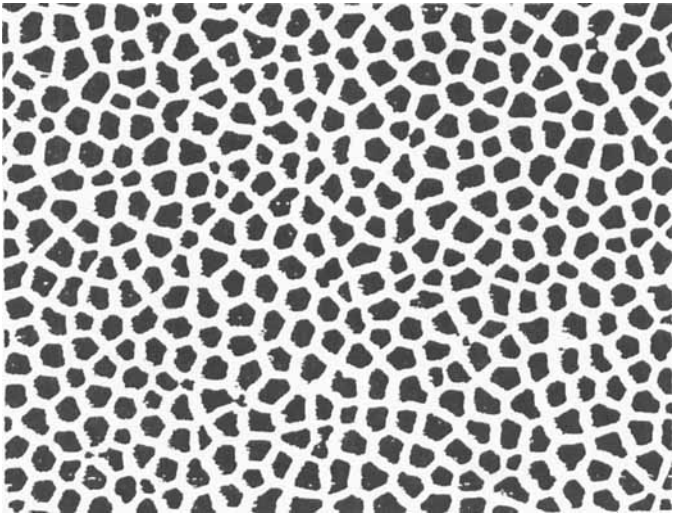

FIGURE 1 SEM of an Anotec Cellular Ceramic Membrane. A View of an Inlet face of the Membrane Perpendicular to the Direction of Flow

and with a slight modification to the description can be applied to asymmetric membranes of this type. If we are to describe the structure of cellular ceramic membranes, then it is important that the details demonstrated in the photomicrograph are retained in the model. That is that the sections are irregular external polygons and that they fully tessellate a plane in 2 space. In early models to describe this structure and models, which have been used by the manufacturers, the pores are assumed to be regular hexagons fully tessellating a plane (1,2). This is clearly not true when one examines the photomicrograph.

Sintered Ceramic Membranes

A typical photomicrograph of a sintered ceramic membrane is shown in Figure 2. This is much different from the cellular ceramic membrane in that now the material is made up of an assembly of spheres which are packed

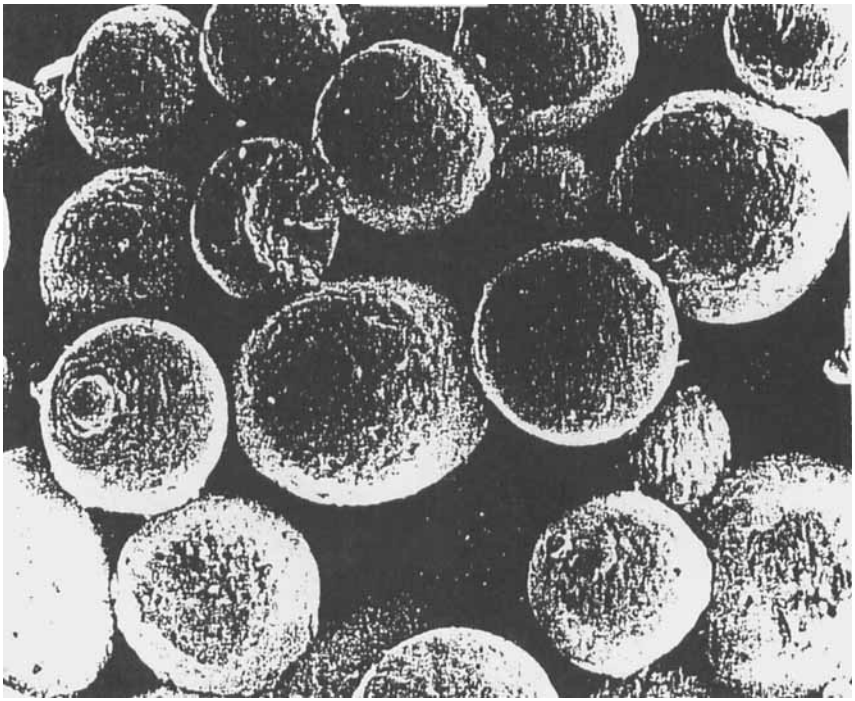

FIGURE 2 SEM of a Sintered Ceramic Membrane

together in a matrix assembly. There are several points of contact between a particular sphere and it's neighbours to produce a stable structure. The sintering process tends to weld adjacent spheres together. The pore space is formed by the voids between the spheres of the matrix. Unlike the cellular membrane, the structure must now be described in 3 space. One similarity between the cellular membrane and the sintered membrane is that symmetric structures can be produced as well as asymmetric structures. In the symmetric structure the particle size distribution of the ceramic beads making up the membrane is constant throughout the material. This leads to a similar pore space through the material. The word 'similar' is used since of course there will be variations within the pore space caused by the

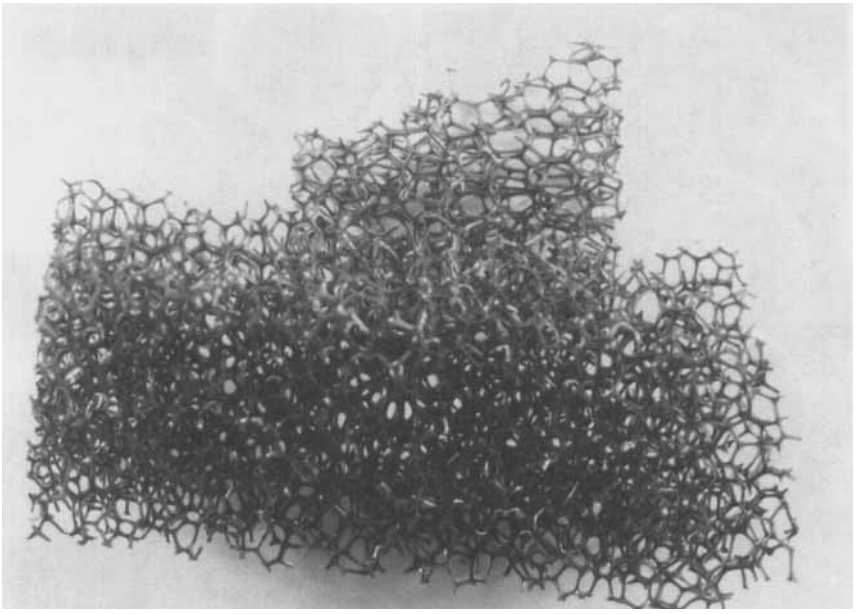

FIGURE 3 Photomicrograph of a Section of a Ceramic Foam Membrane

distribution of particles of the base material. In terms of a statistical distribution the material is, however, homogeneous. In asymmetric sintered membranes a different particle size from the base beads are used at one face of the membrane. Thus the pore space will vary across the membrane in the z direction. The membrane is now heterogeneous. In both cellular ceramic and sintered membranes, the object of using asymmetry is to reduce the cut–off size of the membrane or reduce the average pore cross section area at one face. Conventionally this face is used as the inlet of the membrane.

Ceramic Foam Membranes Used For Micro Filtration

A typical SEM of a cellular foam membrane is shown in Figure 3. This media is used in micro filtration particularly for the filtration of fluids

at high temperatures, an example would be the filtration of molten metals, such as aluminium and stainless steel, to remove slag. These membranes are made using a polymeric foam precursor. Usually reticulated polyurethane foam is used. One method of making these membranes is to compress the polyurethane foam and then immerse it under a ceramic slurry. The compression of the foam is then released which causes slurry to penetrate into the foam structure. The material is then withdrawn from the slurry bath and excess slurry allowed to drain. The polyurethane foam is thus coated with a film of ceramic slurry and it is then placed in a furnace where the ceramic material is sintered. During this process polyurethane foam material is burned off to leave a matrix of ceramic which mimics the structure of the original polyurethane foam. In this way a ceramic foam is produced. Immediately if one examines the photographs one can see that the material is quite different to either of the other two. One similarity with the sintered ceramic material is that now the structure is again a three dimensional structure and must be described in terms as a model of 3 space. Detailed examinations of ceramic foams usually reveal that the cross section of the individual cells formed by the inter–connecting ceramic films are different in one plane to another. In this way they may be described as asymmetric. This asymmetry is a result of the method of manufacture of the original base foam material. Reticulated polyurethane foams are usually made by expansion of a gas bubbling through a liquid polymer solution. This forms a gas liquid foam and as the gas bubbles rise the reduction in hydrostatic pressure results in the individual foam cells being bigger in the vertical plane than in the horizontal. This results in a basic asymmetry which is then transferred to the ceramic membrane during manufacture.

The examination of these three types of membrane reveal some important conclusions. First the individual pores cannot be described by any model based on cylindrical structures. The second conclusion is that the pores are irregular in all cases and cannot therefore be described adequately by any single linear dimension such as a mean pore diameter. Third, the irregular shapes are characteristic of each of the three different structures.

Therefore any models to describe these structures must reflect the basic irregularity of the pore space and must include the basic properties of each structure. In the case of the Anotec cellular ceramic membrane, the basic structure to be reflected in the model must be that the cross section of the pores have the shape of irregular external polygons. These polygons tessellate the total area. Models to represent both the sintered membrane and foam membrane must be described in 3 space. Clearly two different models must be used for these two membranes. In the case of the sintered membrane, the model must relate to random packing of spheres (or near spherical particles) and in the case of the foam membrane, the model must describe the structure of a basic foam. The foam cells form external irregular polyhedra and these again fully tessellate 3 space.

STOCHASTIC MODELS TO DESCRIBE THE STRUCTURE OF THESE MEMBRANE MATERIALS

Cellular Ceramic Membranes

In order to arrive at a suitable statistical model to describe the structure of any porous material one must first consider the physics underlying the method of manufacture of the materials, this can give guidelines to a basic physical model to describe the structure. If we consider the cellular ceramic membrane this, as described earlier, is produced by the electro–oxidation of aluminium. The basic oxide film which is formed on the surface of the metal is nucleated at various points on the surface of the aluminium. The nuclei represent points of high current density and from these the basic pores are formed. As the oxide film first forms on the surface the site described is circular. The nuclei sites on the surface are randomly distributed over the surface and usually result at points where there is microscopic protrusions on the surface. If it is assumed that the nuclei centres of the pores are randomly dispersed across the surface and if they are independent of one another then these centres can be described by a homogeneous Poisson point process over the surface in 2 space. This basic

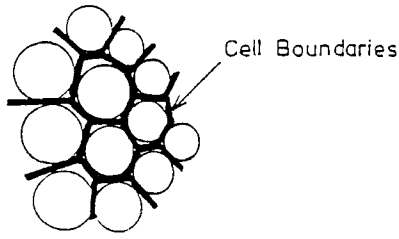

FIGURE 4 Pore Growth Along Lines of Contact On A Simulation Of A Cellular Ceramic Membrane

assumption will be used to develop a pore model to describe the structure. As the pores grow from the nuclei centres, as a result of oxidation, when neighbouring pores expand and ultimately touch, it will be assumed that they then continue to grow along the line of contact. If the oxidation process is continued so that the pores continue to expand, ultimately all the pores will be in contact with their nearest neighbours. The growth process then would cease when the whole surface is oxidised and the resulting cells would form irregular external polygons. The basic statistical process of tessellating 2 space in this way is known as a Voronoi tessellation (3). An example of the growth process showing the boundary between adjacent cells is shown in Figure 4. When an oxide film is formed, the cell boundaries will take the shape shown in this Figure by the lines of contact between adjacent cells. It can be seen from this that the network produces a set of external polygons.

In order to translate this basic physical model into a mathematical algorithm, to simulate the structure of the material, the following sequence is adopted.

First the simulation area A is defined. This is described in terms of dimensions x and y and for convenience positions on this surface are described in terms of dimensionless co–ordinates x^1, y^1 where x^1 is given by $^x/X$. By using dimensionless co–ordinates to define any position in the surface in 2 space the dimensionless parameters x^1 and y^1 will take on values:

$$0 \leq x^1 \leq 1 \qquad (1)$$
$$0 \leq y^1 \leq 1$$

X and Y are the linear dimensions of the area of membrane simulated.

In order to define the number of cells or pores which will be produced on the surface, either the free area, E_a, or porosity, E_v, of the membrane must be specified. Alternately the pore density, that is the number of pores per unit, must be specified. If the free area or porosity is used then a calculation is made in order to calculate the pore density. In this discussion we will assume that the pore density λ is defined. The simulation procedure then follows directly from these definitions. First a set of λ x A points are defined in the simulation area to conform to a Poisson point process. To do this, if we consider first pore one the position of the centre of this pore x^1_1,y^1_1 are defined in terms of a uniformly distributed random variable r, $0 \leq r \leq 1$. r is defined using a random number generator so that this is first used to define x^1 and then a second random number is generated corresponding to y^1, the random number lying in the range of $0 \leq r \leq 1$. These co–ordinates which define the centre of pore one are then stored and the process is repeated for pore two. The co–ordinates x^1_2, y^1_2 are then stored. This procedure is then repeated from i = 1 to i = λ x A and in each case the two co–ordinates are stored along with the pore number. This set of 2 x λ A points then represents the nuclei centres of λ A polygons of a Voronoi tessellation. In order to complete the simulation to produce these polygons one of two procedures may be used. In the first procedure the circles produced from each nuclei centre are allowed to grow at a uniform rate until they touch one or more of neighbouring circles propagated from neighbouring nuclei sites. When two circles touch they are allowed to continue to grow by deformation along the line equi–distant to the nuclei of the touching disks. The growth process is continued until the whole surface has been tessellated to produce a network of polygons. The detailed algorithm to generate this set of polygons although based on a rather simple idea is involved. An alternative procedure is to produce the associated Delauney triangulation of the lattice (4,5). The

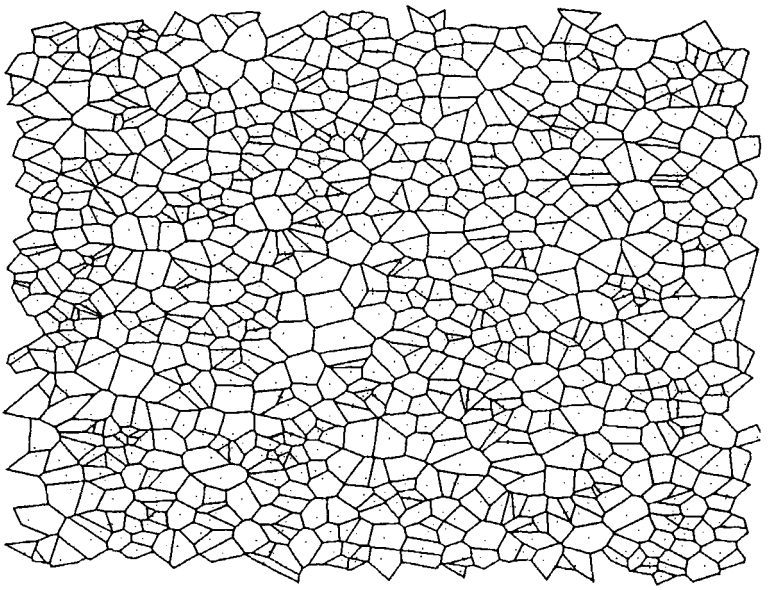

FIGURE 5 Voronoi Tessellation Of 2 Space

Delauney triangulation is related to the Voronoi network and is defined as the network produced by the connection of perpendicular bisectors of sides of the Voronoi polygons. These perpendicular bisectors when connected produce a set of triangles which fully tessellate the space. An example of a Voronoi tessellation is shown in Figure 5. The Delauney triangulation can be produced from the basic Voronoi nuclei points and then from these the Voronoi polygons can be traced.

The result of this model is the definition of a network of external irregular polygons. Mathematically this can be defined in terms of a graph. An important feature of the graph is the co–ordination number at a node, c, that is the junction of walls of neighbouring pores, is a constant, $c = 3$. Apart from the boundary edges of A the graph will fully tessellate the space. A resulting computer simulation from this model is shown in Figure 5. The

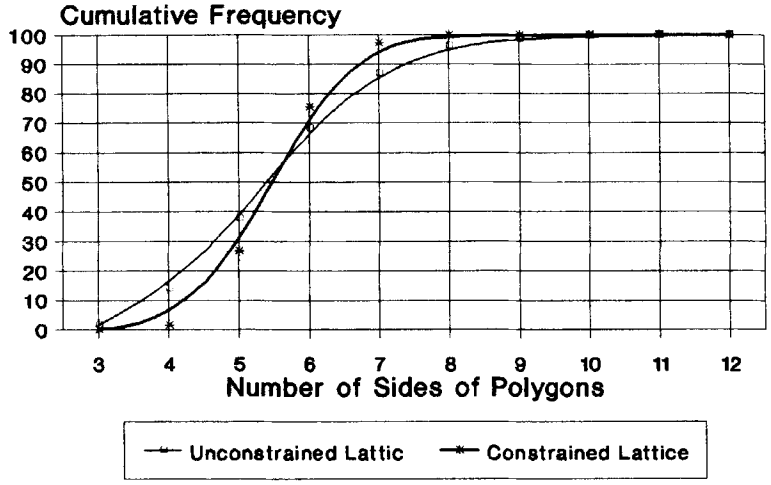

FIGURE 6 Pore Order Distribution Produced By Voronoi Lattices

pores are all external irregular polygons with c = 3. The average number of sides of polygons $\bar{n}$ = 5.9629 with a standard deviation σ_n = 1.3852. If, however, one compares the network with Figure 1, there are some differences. In the simulation there are a number of triangular pores. These are not evident in the SEM of real membranes. The distribution shown in Figure 6 shows that in the Voronoi lattice produced there are some 2% of the polygons with an order, number of sides, of 3. The expected pore area $E(a_p)$ is:

$$E(a_p) = \frac{1}{\lambda} \tag{2}$$

The mean pore order E(n) is given by:

$$E(n) = \frac{2c}{c-2} \tag{3}$$

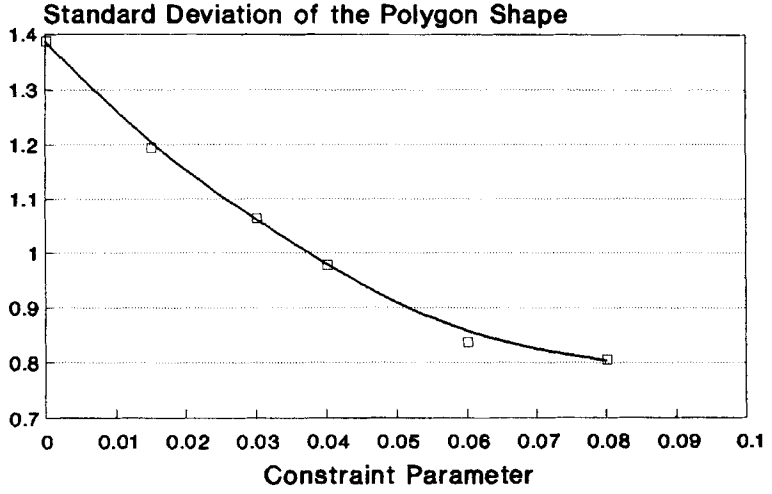

FIGURE 7 Pore Shape Distribution In A Constrained Voronoi Tessellation of 2 Space

Since the Voronoi tessellation c = 3, E(n) = 6. This compares with the value reported above of 5.9629.

The differences in the model structure shown in Figures 5 and 1 can be addressed by introducing constraints to the positioning of the nuclei defining the lattice points, x^1_i and y^1_i. If we introduce a minimum separation distance allowable between neighbouring lattice points, β, such that for nucleus i:

$$\beta_{ij} \geq \sqrt{(x_i - x_j)^2 + (y_i - y_j)^2} \tag{4}$$

for j = 1 ... i − 1, i + 1 ... N.

This will modify the lattice. The effect of this on the pore order distribution, plotted here in terms of the second moment, is shown in Figure 7. The second moment, σ_n, decreases as

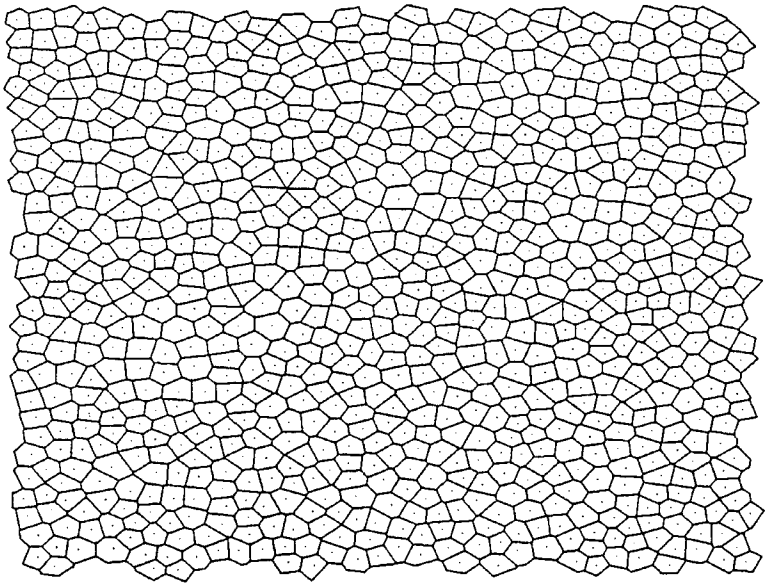

FIGURE 8 A Contrained Voronoi Tessellation Of 2 Space To Simulate A Cellular Ceramic Membrane

β increases. A value of β is reached where the fraction of order 3 pores (triangular pores), F(n=3) becomes zero. This value for β was used in defining the constraint limit. The network produced at this limit on β, $\beta = \beta_{crit}$, was analysed, in terms of the pore order distribution the first and second moment were calculated. The first moment remains unchanged at $E(\overline{n}) = 5.9629$, the second moment decreases to $\sigma_n = 0.8042$. The graph produced of the lattice is shown in Figure 8. SEM photomicrographs of the type shown in Figure 1 were analysed on a digitising image analyser.

The experimental data for pore order are shown in Figure 9. It can be seen from this that there is close agreement between the constrained Voronoi lattice and the experimental results.

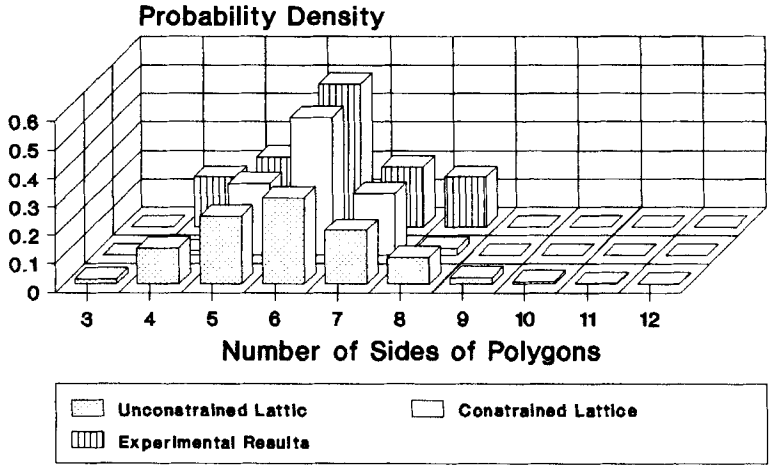

FIGURE 9 A Comparison Between The Pore Order Distribution Produced By The Model With Experimental Measurements

In both Figures 5 and 8 the wall of the pores are simply shown as thin lines. This is, of course, not the case in practice when δ, the wall thickness, is finite and in relation to the diameter of the inscribed circle of a polygon (pore) significant. The area in a unit section of membrane occupied by the pore walls, A_W, is:

$$A_W = \frac{A - A_{pore}}{A} = 1 - A_E \tag{5}$$

where A pore is the total cross section of the pores within the area A. In a unit area of A:

$$A_p = \sum_{\ell=1}^{\lambda} a_{pi} \tag{6}$$

where a_{pi} is the cross section area of pore i, A_E is the free area of the

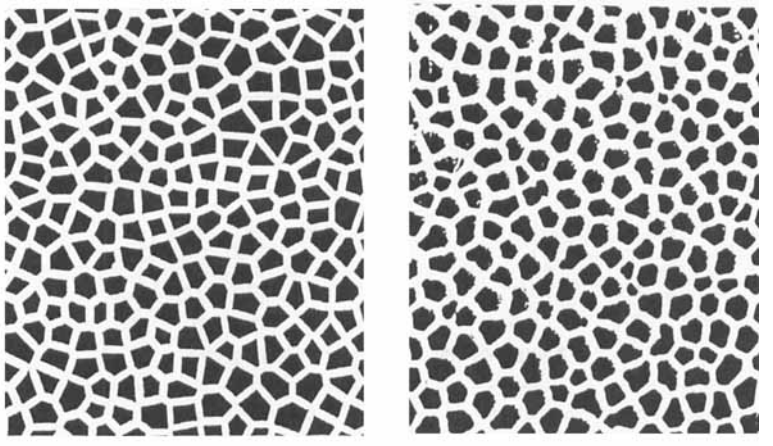

FIGURE 10 A Comparison Of The Structure Of A CCM Membrane Predicted By The Model, a, with experiment, b

membrane. To present a direct comparison between the simulation and real membranes, measurements were made with the image analyser to determine A_E from Figure 1. For a 0.2 μm nominal pore rating Anotec membrane A_E ~ 0.591. This was used to determine $\bar{\delta}$ and the value inserted into the simulation. Thus the simulation model has used two pieces of data taken from measurements of an actual membrane; λ and $\bar{\delta}$. Using these values the structure simulated by this 2 dimensional stochastic model for a C.C.M. membrane is shown in Figure 10. There are some minor differences. At the node points the model produces as a clearly defined angle whereas in practice, because of surface tension forces acting within the electrolyte in the pore during formation, a curved boundary is produced. This can easily be included in the model. Additionally the manufacturing process sometimes results in very brittle walls between adjacent pores. These sometimes rupture during separation and handling to produce a conjugate concave polygon (pore). Some examples are seen in Figure 10b. Comparisons of 10a and 10b produce identical values for c, c=3 and very close values for $E(\bar{n})$: $E(\bar{n})_{SIM} = 5.9629$, $E(\bar{n})_{EXP} = 5.957$. The

frequency distributions for other pore properties; pore area $F(a_P)$, pore perimeter $F(_P)$ and pore hydraulic diameters $F(d_{H_P})$ are shown in Figures 11a–c.

The comparisons of results predicted by the model with measurements from an actual membrane structure are favourable. The sequel to this is can the model be used to predict any performance data of a membrane in use and how do the predictions then compare with experimental data? Two simple cases have been considered. The first is the prediction of clean solvent flux with the applied trans–membrane pressure differential, V vs ΔP. This, although very important in practice, is perhaps not such a sensitive test of the model since if the free area A_E is matched, ΔP is a function of the pore perimeter, p, but will not change dramatically with p.

For laminar flow through the membrane the volume flux is given by the equation:

$$V = \frac{\Delta P}{(32 \ \mu \ell \ A_E)} \cdot \frac{\sum_{i=1}^{\lambda} a_i \, d_{H_i}^2}{\sum_{i=1}^{\lambda} a_i} \qquad (7)$$

where ℓ is the thickness of the membrane. This equation is applicable only to symmetric membranes in which the pore cross section is constant with ℓ.

Since $F(d_H)$ is known and $a_i \, d_{H_i}$ then equation 7 can be solved. The simulation term, ST, is available from the model, A_E and ℓ is also known so that:

$$V = \left(\frac{\Delta P}{\ell}\right) \left(\frac{ST}{A_E}\right) \left(\frac{1}{32\mu}\right) \qquad (8)$$

if $\frac{ST}{A_E}$ is computed = K_m the volume flux can be calculated and if this is

a

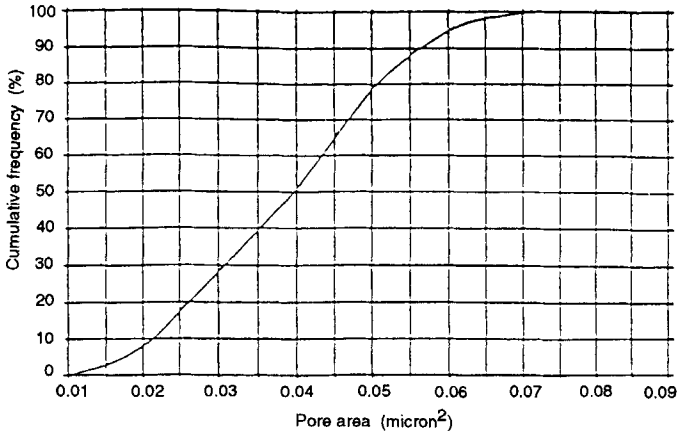

b

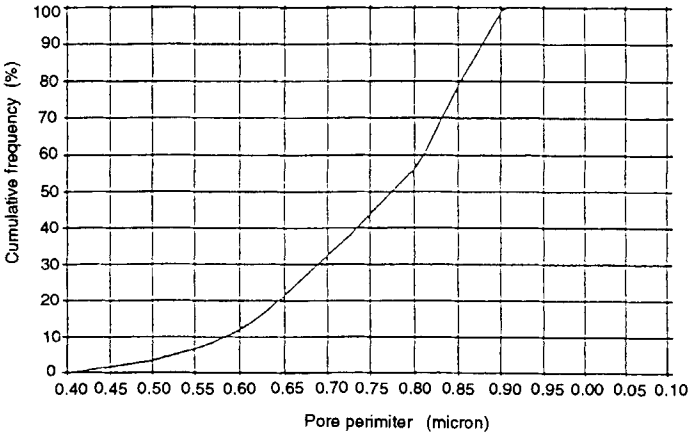

c

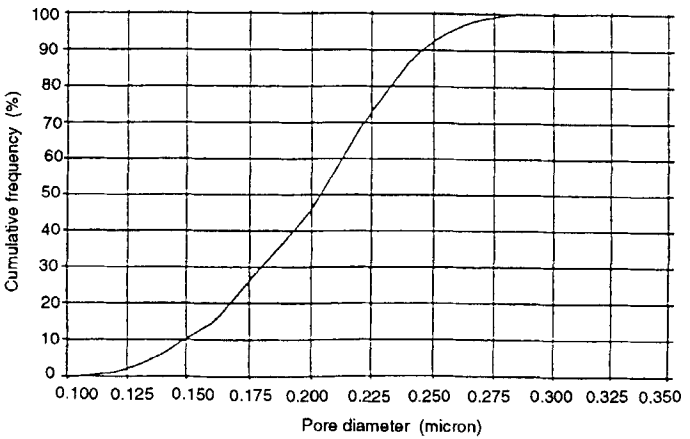

FIGURE 11 Pore Statistics Produced By The Model. a pore area, b pore perimeter, c pore hydraulic diameter

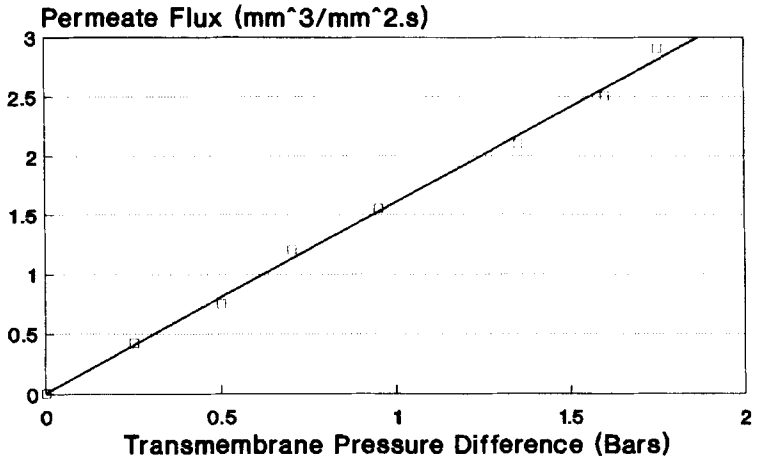

FIGURE 12 Comparison Of The Water Flux Through The Membrane With Transmembrane Pressure Drop

plotted against ΔP a straight line should be obtained passing through (0, 0) with a slope of $(\frac{K_m}{32\mu\ell})$.

Data is shown in Figure 12 for water flux and a 0.2 μm Anotec membrane.

A more sensitive test would be to predict the flux decay with time at a constant trans–membrane pressure as the membrane blinds. The mechanism of blinding in complex and depends on the nature of the material present in the permeate fluid. We will consider an ideal case used by manufacturers when determining and quoting so called 'cut–off' pore size. Here the membrane is challenged with a slurry of carefully sized latex particles dispersed in a solvent. Experiments were carried out in the present work with dilute suspension of latex beads in water. The latex size fraction was chosen so that particles would be close to the pore dimensions. Then if $d_{part} < d_{ci}$, where d_{ci} is the largest inscribed circle of a pore, i, the particle

will pass through the pore with the permeate to be entrained. The criteria for defining particle–pore interactions used in the simulation were taken from the work of Rose and English (6). Thus, if $d_{part} > d_{ci}$ then the particle would remain either on the inlet surface and then form a layer (case i), or if $1.1xd_{ci} > d_{part} > d_{ci}$ then the particle would enter the mouth and become wedged, case ii. In each case the effect will be similar, the subsequent flow through pore i would either cease (i) or be greatly reduced (ii). Measurements were made of permeate flux while filtering in dead–end mode a 5% latex suspension of 0.225 μm beads in water. A 0.2 μm Anotec membrane was used at $\Delta P = 0.34B$. In order to compare the flux decline using the stochastic model for the structure of the membrane, the clear water flux was first computed using equation 7. The interaction of particles in the slurry with the membrane pores was then computed using a stochastic trajectory model. First a distribution function is defined to describe the particle size in the slurry. A normal distribution was used with a mean of 0.225 μm and standard deviation of 0.031 μm. The slurry was assumed to be homogeneous so that there is equal probability for particles in the slurry to approach the filter at any point over the inlet area. Plug flow towards the filter surface was assumed. To compute the particle–pore interaction a particle is selected at random from the distribution, say particle 1. The diameter is determined using the central limit theorem:

$$d_{p1} = \bar{d}_{part} + \frac{\sigma_{part}\left[\sum_{j=1}^{\bar{M}} r_j - \frac{\bar{M}}{2}\right]}{\sqrt{\frac{\bar{M}}{12}}} \qquad (9)$$

where r is a uniformly distributed random variable $0 \leq r \leq 1$ and $\bar{M}$ is an integer $\bar{M} \geq 12$.

The trajectory approach of this particle towards the membrane is next defined by selecting its position in 2 space x^1_{p1}, y^1_{p1}. These values are again determined in terms of r, $0 \leq r < 1$, x^1_{p1}, y^1_{p1} define the position on the

membrane surface where the particle arrives. The membrane model is then interrogated to determine the dimensions of the pore nearest to x^1_{p1}, y^1_{p1}, say pore i, diameter d_{ci}. Initially all pores are open and thus the interaction of the particle with the pore is determined by comparing d_{p1} with d_{ci}. If $d_{p1} < d_{ci}$ the particle is allowed to pass through the pore with the permeate and no increase in the hydraulic resistance of the membrane takes place. If $d_{p1} \geq 1.1d_{ci}$ then the particle is retained on the surface of the membrane and blocks the pore to further flow. The total free area of the membrane is then reduced and therefore in equation 7 the term is reduced giving a reduction in the flux. The intermediate condition $d_{ci} < d_p < 1.1d_{ci}$ which leads to particles being trapped in the mouth of a pore, i, is also considered. This again reduces the flux by, in this case partially sealing the pore. The reduction in area of the pore is computed and the term (ST) in equation 7 (ST) is adjusted. The process is repeated choosing another particle d_{p2} and co–ordinates x^1_{p2}, y^1_{p2}. The interaction is computed with the pore at or nearest x^1_{p2}, y^1_{p2} as before and the outcome v.v the flux determined. The procedure is repeated for n particles $n \tilde{} 10^5$. As the membrane starts to foul pores at any position x^1_{pn}, y^1_{pn} will be blocked. When this condition is met particle arriving at this point are processed by considering the conditions of neighbouring pores to this site. If any or all of these are vacant – open – then the particle is allowed to migrate to the pore of largest cross section area offering the path of least resistance to flow. The pore–particle interaction is then computed. If all neighbouring sites are blocked then particles are assumed to form a surface layer on the membrane. In the present work the resistance of this surface layer is ignored with respect to the resistance across the membrane. This is a simplification which would only be valid if the surface deposit is small.

Results for the computations are shown in Figure 13. For conditions when the particle size distribution is quantitatively similar to the pore size distribution the computed data is close to experimental results. The model provides data on the quantity and size distribution of particles entrained through the membrane in the permeate as well as data on the surface deposit and particles blinding the pores. The latter would not be removed by any back flushing procedures.

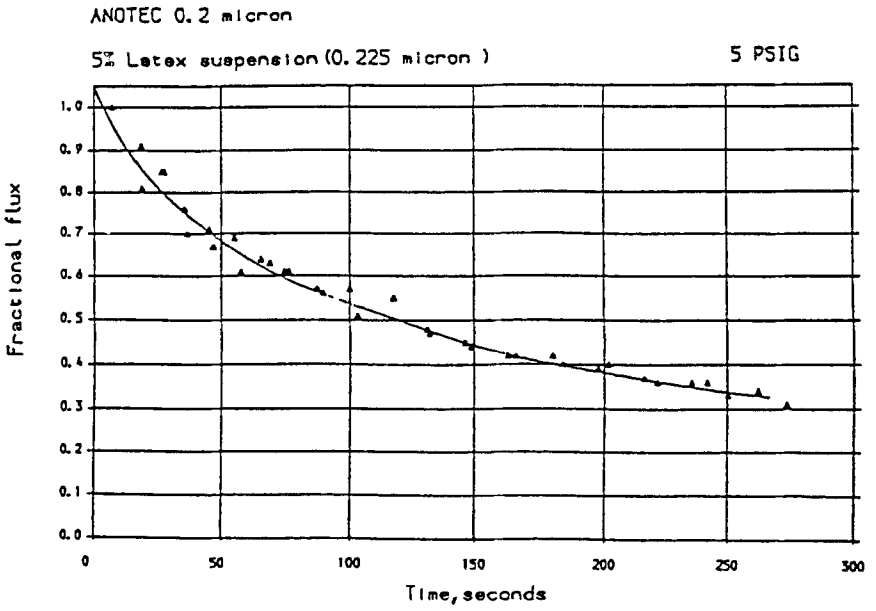

FIGURE 13 Comparison For The Flux Decay With Time At A Constant Transmembrane Pressure Differential, Model Predictions With Experimental Results

Sintered Ceramic Membranes

A major difference between sintered ceramic membranes, ceramic foam membranes and the cellular membranes described in section **3.1** is that these structures can only be described by 3 dimensional models. There is no symmetry or structural similarity in the third plane as in the cellular configuration. SEM photographs show the structure of sintered membranes to be formed from an array of near spherical particles which are fused together at the points of contact. The particles are polydispersed. The basic problem to model is a configuration of nested polydispersed spheres. Although the structure of the cellular membrane described by a pseudo 2 dimensional structure appears at first to have little or no similarity to this problem, there is in fact a considerable common base for both.

If we assume that the relative positions of particles in the basic structure are statistically independent, then one approach is to assume that the centres of the spheres making up the structure are distributed in 3 space by a Poisson point process. As in the previous example the particles can be constructed from these points by a uniform growth process until each particle touches a neighbouring particle, the essence of a Voronoi tessellation in 3 space. The number density of the points distributed in 3 space will then define the average particle diameter. In this simple description the particle size distribution and free volume of the resulting structure will be determined by the site number density and spacial distribution.

To develop a model based on these assumptions, the number density per unit volume, λ_v, is first defined. The sample space, X, Y, Z, is then made non–dimensional by defining the parameters $x^1 = {}^x/X$, $y^1 = {}^y/Y$, $z^1 = {}^z/Z$. Starting with the position of the first particle the position of the centre are defined in 3 space by determining x^1_1, y^1_1, z^1_1 from a uniformly distributed random variable r, $0 \leq r \leq 1$ as before. The sequence is then repeated for each particle 1 through $N = \lambda_v$ in each case the co–ordinates of the centres of each particle i, x^1_i, y^1_i, z^1_i, are stored. To complete the construction the particles are allowed to grow radially at a constant rate from the nuclei sites (centres) until each particle contacts a neighbouring particle. At this point the growth at the two contacting particles are stopped and the corresponding diameters determined and stored. On completion of this process all particle diameters and positions are known. The free volume of this structure, ϵ_v, can then be computed from

$$\epsilon_v = \frac{V - \sum_{i=1}^{N} \frac{\pi}{6} d_i^3}{V} \tag{10}$$

where V is the sample volume V = X Y Z. When the position of the initial nuclei sites, x^1_i, y^1_i, z^1_i, are uncontrained within the sample space the free volume obtained is high $\epsilon_v \tilde{} 0.8$ and generally much higher than that obtained in commercial samples of sintered ceramic membranes. The results also

demonstrate a wide variation in particle diameters and resulting high standard deviation. To modify the structure and to bring it closer to that of actual membrane materials, a constraint or limit process is applied to the initial Poisson point distribution in 3 space. (The procedure is very similar to that applied earlier in the tessellations of 2 space.) The basic requirements are the same – to reduce the variance, in this case the volume, of the unit cells constructed from the Poisson points.) The technique is to generate the N points but as these are defined the distances of all surrounding points are computed and compared to a minimum set value – constraint distance δ. For point i all surrounding nearest neighbour points say k, l, m, n are determined and the distances l–k, i–l, etc computed:

$$\delta_{lk} = \sqrt{(x_i - x_k)^2 + (y_i - y_k)^2 + (z_i - z_k)^2} \qquad (11)$$

δ_{ik} is then computed to δ. If $\delta_{ik} > \delta$ then the distance δ_{il} is computed and so on. If all values exceed the value of δ then condition for point i is accepted. If any one or more distances $\delta_{ik} < \delta$ then the point i is invalid and replaced. As δ is adjusted the free volume of the final structure ϵ_v is modified. A summary of results produced based on a simulation of a membrane sample made up of 8000 spheres are shown in Figure 14. As the constraint distance δ is increased ϵ_v decreases and $\bar{d}$ increases. The simulated structure of the membrane produced by the model are shown in Figures 15a and b. Figure 15a shows a close up of the structure seen normally to a face of the membrane. In Figure 15b a sample volume is rotated to show the 3 dimensional packing structure.

The constraint Poisson point process model introduces a minimum pair separation to the normal unconstrained process to control the mean size and size distribution of the individual spheres making up the structure, obviously the greater the value of δ the larger the mean size and the smaller the range of the distribution. However, as the points are introduced randomly, as δ is increased the computer time spent in generating a given number of points within a simulation volume increases. There is an upper limit for packing of hard spheres using this minimum pore separation

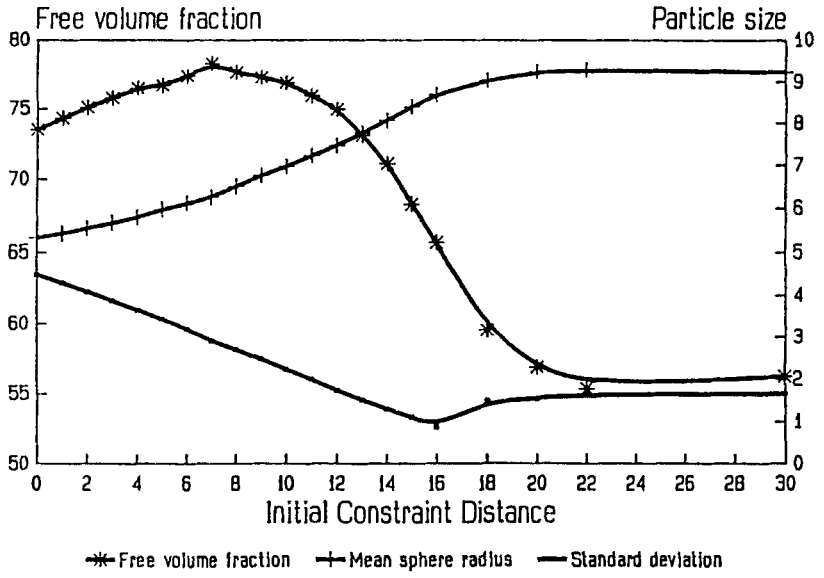

FIGURE 14 Variation Of Free Volume With Interparticle Spacing

concept. Alternative procedures can be adopted all based on the same concept of utilising a Poisson point process in 3 space to define the positions of hard spheres but applying different rearrangement algorithms to control ϵ_V. Two other methods have been employed in the present work; (i) an expansion model and (ii) a vibration model. In the expansion model the algorithm expands and/or moves adjacent spheres according to a set of deterministic values rather than randomly. The idea is to achieve a more stable highly packed structure. According to the expansion model if a sphere is in contact with another sphere it will expand itself along the line of centres until it contacts a second sphere. If it is already in contact with two spheres it will grow until it touches a third sphere whilst maintaining contact with the other two. Further growth is possible from this position, if it is in contact with three spheres but its centre is not on the plane defined by the centres of the three contact spheres it can expand again until it contacts a fourth sphere. It can expand again if it has four contact spheres but the

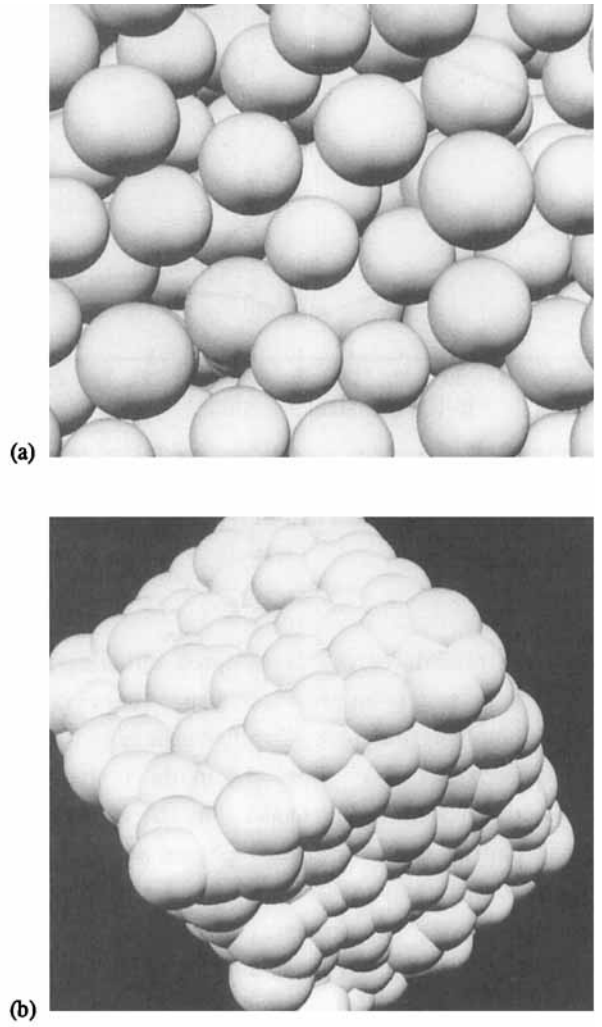

FIGURE 15 A Section Of A Sintered Ceramic Membrane Predicted By The Model

centre is outside the tetrahedron formed by the centres of the four spheres growth can continue until it contacts a fifth sphere, etc. This series of modifications can be implemented in a fast efficient algorithm to obtain high packing densities and low free volumes ϵ_v. The modification rules necessarily affect the size distribution of the resulting spheres.

In the vibration algorithm the procedure is effectively reversed. First the size of the spheres is predefined according to some distribution function, such as for example equation 9, and the position of the individual spheres are generated randomly. This procedure will inevitably contain a large number of overlaps. The vibration algorithm, effectively eliminates the overlaps according to a set sequence. To minimise the chance of introducing new overlaps as ones are removed the procedure starts with the most serious overlap. The order of overlap is chosen using the term Δ_i.

$$\Delta_i = \Sigma I_{ij} \, (A_{ij}^2 - B_{ij}^2) \qquad (12)$$

$$l, j = 1, 2, 3, \ldots N$$

where $I_{ij} = 0$ if j overlaps with i

$I_{ij} = 1$ if no overlap exists between j and i.

A_{ij} is the minimum pair separation allowed and B_{ij} is the computed distance. The larger Δ_i the more serious the overlap. A summary of the properties of the structures and computational efficiency of these three methods are summarised in Table 1. From this work it is recommended that the expansion algorithm is used to simulate the structure of sintered ceramic membranes. Having matched ϵ_v between the model and the experimental structure the detailed pore structure can be computed, in this case the pores are formed by connected pathways formed in the space between touching particles – a series of convergent divergent channels. Particle retention within the membrane can be simulated by a procedure similar to that outlined in section 3.1 for two cases, (i) the case when $\bar{d}_{part} <<$ pore minimum cross section diameter. This work has been considered by Rowley (7).

TABLE 1 Comparison Of The Random Packing Algorithms

Name	Description	Feature & Comment
Constraint Poisson Point process model	First generate an assembly of points then let points to grow into spheres Use a minimum pair separation	Stochastic algorithm Slow at large minimum pair Indirect control of the size distribution Low co–ordination number
Expansion algorithm	Expands spheres in a given configuration to maximise size and co–ordination number	Analytical algorithm Very fast Affects size distribution Efficient to obtain high packing density
Vibration model	Elimination overlaps in a configuration of a given nominal packing density Need to determine the most serious overlap(s) at each MC iteration	Analytical algorithm Extremely slow Does not affect size distribution Capable of generating the maximum packing density

Ceramic Foam Membranes

The underlying structure of the foam can be produced by an extension of a Poisson point process in 3 space if it is assumed that the centroids of the polyhedral cells of the foam are spacially independent. The extension is similar to the construction of a Voronoi tessellation of 2 space from a Poisson point process in 2 space. In other words a model for the ceramic foam membrane can be viewed as an extension of the basic model of the sintered

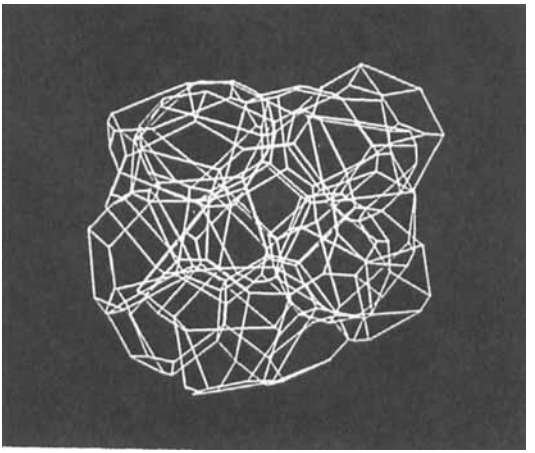

FIGURE 16 A Section Of A Cellular Ceramic Foam Membrane, Predicted By The Model

membrane and is related, although a higher order, to the 2 dimensional model described for a cellular membrane.

If the cells in a constrained Poisson point process in 3 space are allowed to expand and, when adjacent cells touch, growth is continued along the plane of contact until the volume space is completed tessellated a set of Voronoi polyhedra will be produced. This structure can be used to simulate a ceramic or polymeric foam. To do this only the edges of the faces of the polyhedra are displayed, Figure 16. These represent the cell connections of the membrane. Examples of the resulting structure are shown in Figures 17a and 17b diagrams the line thickness of the various edges are allowed to vary. This is seen in the real material and is a result both of variation in the thickness of the underlying polyurethane base foam and the variation in drainage of slurry driving the manufacturing process. The 3 dimensional Voronoi tessellation can be analysed to produce statistics on the properties of the polyhedra. First the co–ordination number of any lattice point in the graph is 3. This is as experienced in actual membrane materials. If in any

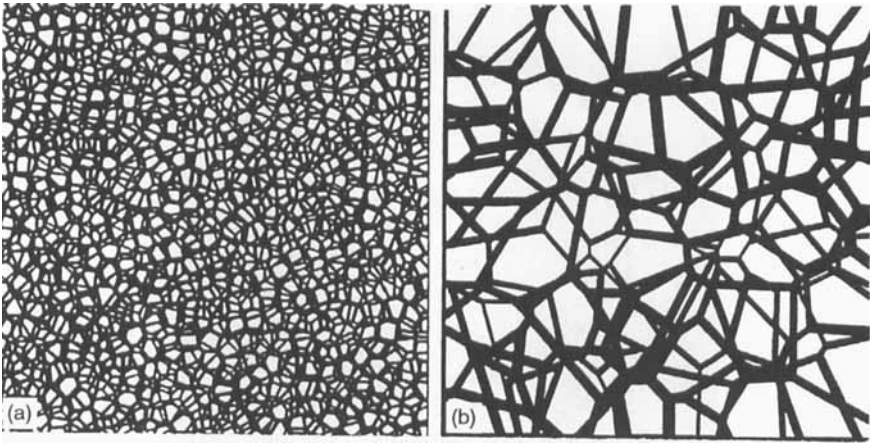

FIGURE 17 A Model Of A Foam Membrane Based On A Voronoi Tessellation In 3 Space

polyhedra i the volume is V_i, the number faces Nf_i, the number vertices is Nv_i, the number of edges is Ne_i then from the computations the expected values of these parameters in the network, E ( ) are:

$$E(V) = \frac{1}{\lambda} \tag{13}$$

$$E(Nf) = 14.3636 \tag{14}$$

$$E(Ne) = 37.0909 \tag{15}$$

$$E(Nv) = 24.727 \tag{16}$$

The comparison between the predictions of the structure of the membrane from the model and the actual material is good. The basic structure of the graph compared to the actual material is correct. It was pointed out earlier that the average dimensions of cells in a foam membrane are statistically anisotripic and are larger in one direction than the other two orthogonal directions. This is due to the expansion of gas bubbles during manufacture. This can be readily incorporated into the model by carrying

out a linear affine transformation in one plane. This transformation can be expressed:

$$W:R^3 \rightarrow R^3 \tag{17}$$

$$\begin{bmatrix} x^1 \\ y^1 \\ z^1 \end{bmatrix} = \begin{bmatrix} 1\,0\,0 \\ 0\,1\,0 \\ 0\,0\,a \end{bmatrix} \begin{bmatrix} x \\ y \\ z \end{bmatrix} \tag{18}$$

When this transformation is included in the model the conditions observed in a foam membrane can be modelled with accuracy. The transformation will not influence the properties defined in equations 13 and 16 but will, of course, alter the perimeter of the cells and the area of the faces or apertures in the membrane structure through which the fluids must permeate.

CONCLUSIONS

Deterministic models cannot be used to represent the properties or structure of porous membrane materials. The material structure of these are not uniform either in shape, area or volume. Models to simulate the structures observed in membrane materials should be based on stochastic geometry. This concept has been applied to simulate the structure of three different types of ceramic membranes which cover an important range of industrial membrane materials. The three structures, although appearing quite different, can in fact be described by one generic model based on a homogeneous random division of space. The cellular ceramic membrane manufactured by electro–oxidation of aluminium is essentially a 2 dimensional structure and can be successfully modelled by a Voronoi tessellation of 2 space. The other two types of membrane considered, the sintered ceramic membrane and foam membrane, are 3 dimensional structures. These can both be modelled by a similar technique if the tessellation is taken into 3 space. Variations of these statistical models can

be performed to represent asymmetry and to represent measured changes in free volume. The models can provide detailed statistical data on the pore properties and can be used to compute permeate flow and particle retention.

NOMENCLATURE

L = length, M = mass, T = time

A	area	L^2
A_E	free area	–
A_{ij}	minimum pore separation distance	L
A_p	sum of the cross section area of pores	L^2
A_w	cross section area of particles of pores	L^2
a_i	cross section area of pore i	L^2
a_p	cross section area of pore	L^2
B_{ij}	computed distance between pores i and j in 3 dimensional space	L
c	coordination number of a mode	–
d_{ci}	diameter of the largest inscribed circle of pore i	L
$\bar{d}_{part}$	mean particle diameter	L
d_{part}	particle diameter	L
d_H	hydraulic diamater of a pore	L
$E( )$	expected value of a function	–
E_n	free area of a membrane at the inlet face	–
E_v	free volume of a membrane	–
$F( )$	function	–
I_{ij}	conditional parameter on pore position eqn (12)	–
ℓ	length of a pore in the direction of permeate flow	L
M	intiger number ≥ 12	–

N_{ei}	number of edge of a pore	–
N_{fi}	number of faces of a pore	–
N_{fi}	number of vertices of a pore	–
n	number of sides of a polygon	–
ΔP	pressure drop	ML^{-2}
r	uniformly distributed random number $0 \leq 1 \leq 1$	–
v_i	volume of pore i	L^3
v	volume	L^3
V	volume flow of permeate	$L^3\ T^{-1}$
x,y,z	Cartesian coordinates	
x^1,y^1,z^1	dimensionless coordinates	
X,Y,Z	linear dimensions of a membrane in direction x, y, z respectively	L
$x^1_{p1},y^1_{p1},z^1_{p1}$	dimensionless position coordinates of particle 1	
β	minimum separation distance by nucleic points in 2 dimensional space	L
β_{oit}	critical minimum separation distance of 2 nuclei points in 2 dimensional space	L
β_{ij}	distance between the nuclei of pores i and j	L
δ	wall thickness	
δ_{ik}	distance between pores i and k in 3 dimensional space	L
δ	constraint distance of nuclei in 3 dimensional space	–
ϵ_v	free volume of a membrane	–
λ	number density of pores in 2 dimensional space	–
λ_v		
μ	viscosity of permeate liquid	$ML^{-1}T^{-1}$
Δ_j		
σ_p	standard deviation of the diameter of pores	

ACKNOWLEDGEMENT

The Authors would like to thank AEA Technology, Anotec Limited and British Nuclear Fuels PLC for financial support and encouragement to carry out this work.

REFERENCES

1 G.E. Thomson, R.C. Furneaux, J.S. Goode and G.C. Wood, Trans. Inst. Metal Finishing, 56, 159 (1978).

2 R.C. Furneaux, W.R. Rigby and A.P. Davidson, Nature, Vol.337, p. 147 (1989).

3 R.E. Miles, Math. Bio. Sciences, 6, 85–127 (1970).

4 A.L. Hinde and R.W. Miles, J. Statis. Comput. Simul., 10, 205–223 (1980).

5 D.F. Watson, The Compution Journal, 24, 167 (1981).

6 H.E. Rose and J.E. English, Trans. Inst. Chem. Eng., 51, 14 (1973).

7 M.E. Rowley, PhD Thesis, University of Manchester (1989)

8 N.M Jackson, MSc Dissertation, University of Manchester (1991).